Onboard Navigation Error Analysis for Aerocapture at Uranus

Pardha Sai Chadalavada*
Analytical Mechanics Associates, Hampton, VA 23681, USA

Rohan G. Deshmukh*, Rafael A. Lugo*, Soumyo Dutta†
NASA Langley Research Center, Hampton, VA 23681, USA

Lylia Benhacine*
Draper Laboratory, Houston, TX 77058, USA

Declan Mages*
Jet Propulsion Laboratory, Pasadena, CA 91109, USA

Capturing into an orbit around Uranus using aerocapture allows one to design a mission with faster interplanetary trajectories and less propellant requirements. Such an aerocapture mission would rely on the onboard Guidance, Navigation, and Control (GNC) subsystems to successfully capture into an orbit around Uranus. Uncertainty in the state information and the noise in the sensor measurements induce navigation errors in the guidance and control subsystems, which can affect the overall performance of the aerocapture mission at Uranus. Understanding the effect of these navigation errors on mission performance is essential. To this end, this work considers different sensors with varying quality to understand their impact on the overall mission performance. In addition, this paper studies the impact of the uncertainty in the initial states used to initialize the onboard navigation filter and understands their effect on mission performance. This paper also shows the onboard navigation errors obtained from the Linear Covariance (LinCov) analysis and uses them for verification and validation (V&V) of the results from Program to Optimize and Simulate Trajectories-II (POST2).

I. Introduction

Aerocapture utilizes a planet's atmosphere to dissipate energy when arriving from a hyperbolic orbit to get captured into an orbit around the planet [1–3]. The performance of the aerocapture depends on several factors such as atmospheric uncertainties [4, 5], aerodynamic uncertainties [6, 7], and navigation errors [8, 9]. One can further classify the navigation errors into interplanetary and onboard navigation errors. This work mainly focused on the onboard navigation errors during the aerocapture at Uranus.

The source for the onboard navigation errors is the initial navigation error in the entry state used to initialize the onboard navigation filter and the onboard navigation errors accumulated during the aerocapture trajectory due to the propagation of the Inertial Measurement Unit (IMU) sensed measurements, which are corrupted with noise. The onboard filter can mitigate these errors using the measurement updates from other sensors. However, for an aerocapture mission, one can assume that there will not be any additional measurements that the filter can use. Therefore, the filter will only propagate the IMU states with no measurement updates during the aerocapture. As a result, an aerocapture mission's performance depends on the initial states' uncertainties and the quality of the IMU sensors. To this end, this paper considers uncertainty in the entry states used to initialize the onboard navigation filter and multiple IMU sensor models to understand the effect of navigation errors on the aerocapture performance at Uranus.

This work analyzes onboard navigation errors using two techniques: 6 Degrees Of Freedom (DOF) trajectory simulated with onboard navigation modeled in Program to Optimize and Simulate Trajectories- II (POST2), and Linear Covariance (LinCov). The LinCov analysis is used to identify different IMU models that one can use to perform aerocapture and to verify and validate (V&V) the onboard navigation modeling in POST2. The Draper LinCov tool [10] is a linear covariance analysis tool designed to estimate navigation errors and trajectory dispersions for space missions. It has been used across many flight phases and GNC designs. In this paper, LinCov will be used to perform a navigation

*Aerospace Engineer, AIAA Member.
†Aerospace Engineer, AIAA Associate Fellow.

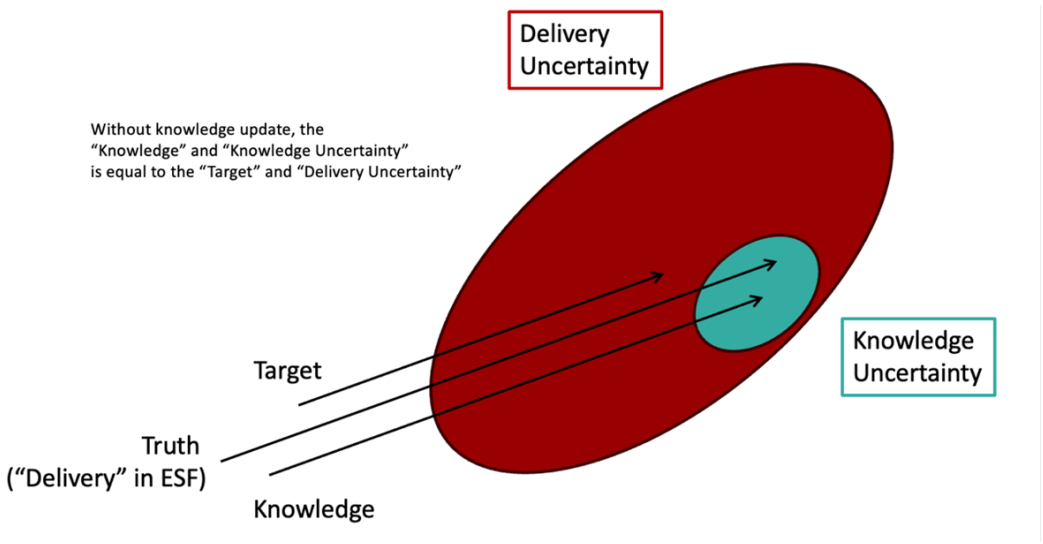

Fig. 1 Visualization of delivery and knowledge uncertainty at targeting entry interface point to start aerocapture

error analysis for the aerocapture trajectory, which is the focus of the POST2 analysis. This will provide validation for the navigation analysis. Specifically, this analysis aims to explore the sensitivity of navigation performance to IMU quality. A similar study was performed for Mars Entry Decent and Landing (EDL) [11].

The rest of the paper is organized as follows: Section II discusses the POST2 and LinCov simulation setup, along with a discussion on how the initial states for the onboard navigation filter are generated. Section III presents the onboard navigation error analysis for the aerocapture at Uranus. The conclusions of this study are presented in Section IV.

II. Simulation Setup

This section will discuss the simulation setup of POST2 and LinCov in detail. In addition, this section also discusses how the initial values of the onboard navigation states are obtained.

A. Initial States

Initial values of position, velocity, and attitude (inertial to body) are required to initialize the onboard navigation filter, which is discussed in detail in Section II.B.2. This section discusses in detail how these initial values are obtained.

1. Position and Velocity

An Entry State File (ESF) provides data related to the state and state uncertainty for entry delivery, using interplanetary navigation analysis techniques. It is a file format with extensive mission heritage. The file is generated using the JPL software Mission analysis, Operations and Navigation Toolkit Environment (MONTE), [12] and contains summary information of the interplanetary navigation solutions followed by N samples of dispersed Cartesian delivery states and N samples of dispersed Cartesian delivery knowledge states, all at the same nominal entry epoch minus 10 minutes. Delivery states represent the range of possible delivered states defined by the spacecraft-Uranus state knowledge at the final maneuver data cutoff plus maneuver execution error. Here, that is 4 days from entry. Knowledge states represent the knowledge of where each delivered state ended up relative to the desired target and is defined by the knowledge data cutoff, which is 16 hours from entry. This includes more data and an estimate of maneuver execution error, and provides a significant improvement on uncertainty versus the final maneuver data cutoff. A depiction of delivery and knowledge uncertainty is depicted in Figure 1. The interplanetary navigation modeling and estimation of these delivery and knowledge uncertainties is given in Restrepo et al. and Mages et al.[9, 13].

2. Attitude

This section discusses how the initial attitude information for the Multi-mode Extended Kalman Filter (MEKF) is generated for the nominal run and the off-nominal runs used for the Monte Carlo analysis. The initial attitude is represented using a quaternion from the MEKF inertial frame to the body frame. The inertial frame of the MEKF is a planet-centered inertial frame locked at the epoch when the MEKF module is initialized in POST2. The initial nominal quaternion from MEKF inertial to the body is obtained from the POST2 truth states. Ref [14] discusses how the POST2 truth attitude states are initialized in detail. In this work, to generate the dispersions of the initial attitude quaternion for the MEKF, first the four elements of the nominal quaternion attitude are converted into three Euler angles. Then, the three Euler angles are uniformly dispersed by 0.15 deg. In addition, the magnitude of the dispersed Euler angles is also uniformly dispersed by 0.05. Using these dispersed Euler angles and their magnitude with additional dispersion, one can compute the dispersed quaternion, which is used as the initial attitude for the off-nominal cases to perform the Monte Carlo analysis.

B. POST2 Navigation Setup

This section discusses the aerocapture simulation run in POST2 [15] to model the onboard navigation errors. The 6DOF simulation setup used to study the onboard navigation errors during the aerocapture at Uranus is discussed in detail in Ref [14]. Figure 2 shows the onboard GNC subsystems modelled in POST2 to simulate the aerocapture at Uranus. Here, we will discuss in detail the onboard navigation subsystem. The navigation subsystem contains the IMU model and the Multi-model Extended Kalman Filter (MEKF), which are discussed in detail below. As shown in Figure 2, the errors in the navigation subsystem are passed on to guidance and control subsystems that will affect the 6DOF aerocapture trajectory and thereby affect the aerocapture's performance.

1. IMU Module

The IMU sensor is modeled using the strap-down IMU module in the POST2. This module can model several IMU errors such as those due to constant bias and scale factor, errors due to non-orthogonality, and noise random walk. In addition, this module allows one to model errors due to quantization. This IMU module can model the measurements from the accelerometer and gyroscope in the form of the change in velocities (ΔV) and change in the angles ($\Delta\theta$). In POST2, one can call the IMU module at a desired frequency. A 200Hz call rate for the IMU sensor is considered in this work. This model takes the truth measurements from POST2 states and adds error terms from different sources discussed earlier to compute the ΔV and $\Delta\theta$ measurements similar to the ones that an actual onboard IMU sensor would provide. This model can generate different error profiles using different random number generation seeds, which is useful to run the Monte Carlo analysis. These measurements are then passed on to the MEKF, where they are integrated to compute the onboard navigation states. These states will be the vehicle's best estimate regarding its current position. To this end, due to the errors in the IMU measurements, the onboard navigation states will not be accurate compared to the true states where the vehicle is flying. The aerocapture performance degrades as the guidance commands and the commands from the control systems (please refer to Ref [14, 16] for more details on the guidance and control subsystems) are generated using the onboard navigation states while the vehicle flies in a different environment, corresponding to the truth states. These onboard navigation errors can impact the aerocapture performance, especially when using a closed loop guidance as shown in Figure 2. However, one can choose an IMU that can provide performance metrics that are sufficient for successfully performing aerocapture. To this end, the sensitivity of the aerocapture performance with respect to the IMU quality is shown in Section III.A. The MEKF that integrates the IMU measurements to generate the onboard navigation states also contributes to the onboard navigation errors and is discussed in detail in the following section.

2. MEKF Module

This section will detail the MEKF module in POST2 that integrates the IMU measurements to generate the onboard navigation states. The MEKF module in POST2 can blend sensor data from multiple sensors such as altimeter, velocimeter, attitude cameras, Deep Space Network (DSN), Navigation Doppler Lidar (NDL), and Terrain Relative Navigation (TRN). However, obtaining data from these sensors is not practical for an aerocapture mission. To this end, in this work, the MEKF integrates the IMU states using the IMU process noise (to account for the uncertainties in the IMU measurements) and does not receive any measurement updates. The MEKF in POST2 has ten primary states: three for inertial position, three for inertial velocity, and four for the inertial-to-body quaternion. The previous section discussed how the initial values for these ten primary states are generated. As previously mentioned, the inertial frame

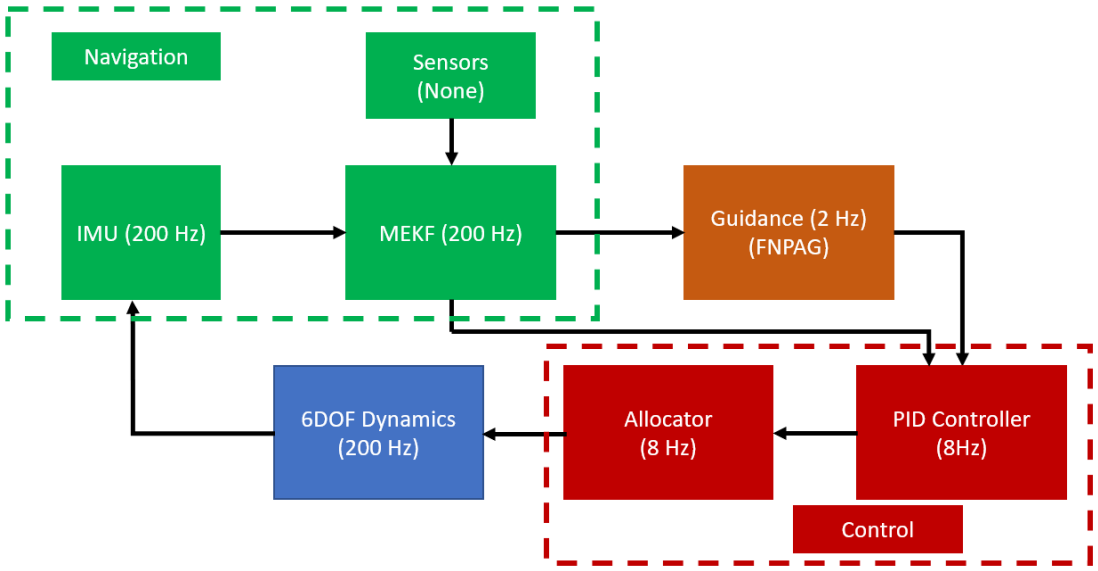

Fig. 2 Aerocapture simulation setup.

of the MEKF is a planet-centered inertial frame locked at the epoch when the MEKF module is initialized in POST2. Similar to the IMU module, one can call the MEKF module at any desired frequency. However, a 200 Hz has been used in this work due to heritage from previous missions. The MEKF module in the POST2 allows one to ignore specific IMU measurements below a threshold, which are considered for sure to be noise. However, in this work, all the IMU measurements are processed to obtain the onboard navigation states. To initialize the MEKF in POST2 in addition to the initial values for the ten primary states, one will have to provide the initial onboard navigation errors covariance (9×9) and the IMU process noise terms (6×6). The first three rows in the error covariance correspond to position, the next three rows correspond to velocity, and the remaining three rows correspond to the attitude. The first three rows of the IMU process noise correspond to the accelerometer, and the remaining three rows correspond to the gyroscope. The previous section discusses the generation of initial states for the MEKF for the nominal case and the off-nominal cases for the Monte Carlo analysis. Ref [14] discusses the initial truth states used to run the nominal and off-nominal 6DOF aerocapture simulations. From ESF, we have 8001 initial truth and navigation states to run a Monte Carlo analysis. The navigation errors are defined as the difference between the onboard navigation states and the truth states from POST2. Using the 8001 onboard navigation and truth states, one can generate 8001 initial onboard navigation errors by subtracting the navigation states from truth states, which are used to create the 9×9 initial onboard navigation error covariance used to initialize the MEKF. The 6×6 IMU process noise terms depend on the quality of the accelerometer and gyroscope modeled. The diagonal terms are computed using the IMU specifications and the remaining terms are considered zero. In addition to POST2 simulation, this work uses LinCov to estimate the onboard navigation errors. The following section will discuss the LinCov setup in detail.

C. LinCov Setup

Three different IMUs are considered for the LinCov analysis: low-, medium-, and high-quality. The assumed specifications for the IMUs are shown in Table 3. Initial navigation states/errors are identical to those assumed for the navigation analysis in POST2, discussed earlier. Guidance and control are assumed to be perfect in this analysis, so navigation errors are driven primarily by the differences in the IMU. That is, the onboard navigation states do not affect the outputs of the guidance and control subsystems. The Uranus Global Reference Atmosphere Model (UranusGRAM2021 [4]) is used for the atmosphere model. For the navigation error analysis in LinCov, an aerocapture trajectory was generated using the Fully Numerical Predictor Corrector Aerocapture Guidance (FNPAG). Key parameters for the trajectory are shown in Table 1. The key parameters are identical to the POST2 simulation.

Table 1 Key parameters used for the LinCov analysis

Parameter	Value
Inertial Entry Velocity	24.9347 km/s
Inertial Entry Flight Path Angle	-11.1034 deg
Atmosphere Model	UranusGRAM2021
Geocentric Radius at Entry	26559.00 km
L/D	0.25

III. On-Board Navigation Error Analysis

In this work, we use the simulation of the aerocapture at Uranus in POST2 to study the affects of the onboard navigation errors. The aerocapture is used to capture into an orbit with a target apoapsis altitude 2 million km and a target periapsis of 53000 km to be above the rings. Table 2 shows the initial states of the vehicle used for this simulation. UranusGRAM2021 is used to model the Uranus atmosphere. Custom aerodatabase and aerothermal database developed for the Uranus atmosphere and Mars2020 like aeroshell vehicle configuration are used. Please see Ref [14] for more details on the simulation setup used in this work to study the onboard navigation errors.

Table 2 Initial states used for the POST2 analysis

Parameter	Value
J2000 Position X-coordinate	7.71224309e+06 km
J2000 Position Y-coordinate	-8.15905635e+06 km
J2000 Position Z-coordinate	2.90309665e+07 km
J2000 Velocity X-coordinate	-1.65892892e+04 km/sec
J2000 Velocity Y-coordinate	1.48590592e+04 km/sec
J2000 Velocity Z-coordinate	-2.35330714e+03 km/sec

A. Navigation Sensitivity Analysis

This section will present the sensitivity of onboard navigation errors to aerocapture performance. As discussed earlier for aerocapture simulation, no measurements are updated to the onboard navigation filter, and errors in the IMU measurements are propagated over time. To this end, this section compares three different IMUs with varying quality. Table 3 shows specifications used to model different IMUs with varying quality, which are the same as the ones used for LinCov analysis. This work considers the high-quality IMU for the baseline simulation. For the rest of this section, we will use this baseline simulation as the reference for different comparisons. This section will first compare the FNPAG [16] bank commands using the bank and onboard navigation states. Secondly, the aerocapture performance obtained using perfect navigation with no navigation errors is compared with the baseline simulation. Thirdly, the sensitivity of the aerocapture performance concerning the IMU quality is presented, followed by the discussion on the sources of onboard navigation errors. Finally, the aerocapture performance of the baseline simulation is compared with the case when the spacecraft does not receive a navigation update 16 hours before the entry.

Figure 3 compares the FNPAG bank commands generated using 1) the onboard navigation states with errors and 2) the POST2 truth states from entry interface to the guidance off trigger. Entry interface is defined as 1000 km altitude, while the guidance off trigger is 0.1 g while the vehicle is exiting the atmosphere. FNPAG uses the current states of the vehicle to compute the bank commands and generate different commands when using the navigation states and the truth states. The vertical lines showing different events during the aerocapture simulation belong to the baseline trajectory. Analysis shows that these events approximately have the same timeline compared to the aerocapture trajectory with perfect onboard navigation. The FNPAG commands are comparable, as shown in Figure 3, showing us that the effect of the navigation errors on the guidance is minimal. For both cases, the initial bank angle (before the FNPAG issues any commands) is 90 deg from the entry interface to the guidance-on event. The FNPAG has an internal rate limiter that commands the smooth bank profiles from 0 deg to 90 deg. Ref [16] discusses the FNPAG in more detail. After the guidance is on, during the first phase [16], FNPAG should be commanding a 15 deg bank. As we can see from

Table 3 Specifications for different IMUs [17]

Specification (3 σ per axis)	High quality	Medium Quality	Low Quality
Gyro constant bias	0.036 (deg/hr)	0.15 (deg/hr)	0.3 (deg/hr)
Gyro constant scale factor	27 (ppm)	15 (ppm)	100 (ppm)
Gyro non-orthogonality	19 (arcsec)	75 (arcsec)	60 (arcsec)
Gyro Random walk	0.015 (deg/$\sqrt{hr}$)	0.018 (deg/$\sqrt{hr}$)	0.21 (deg/$\sqrt{hr}$)
Gyro internal quantization	1.00E-06 (counts to rad)	5.00E-06 (counts to rad)	1.00E-05 (counts to rad)
Gyro external quantization	1.00E-06 (counts to rad)	5.00E-06 (counts to rad)	1.00E-05 (counts to rad)
Accel constant bias	84 (micro-g)	300 (micro-g)	900 (micro-g)
Accel constant scale factor	450 (ppm)	525 (ppm)	900 (ppm)
Accel non-orthogonality	17 (arcsec)	45 (arcsec)	20 (arcsec)
Accel Random walk	0.0003 (m/s/($\sqrt{s}$)))	0.0015 (m/s/($\sqrt{s}$)))	0.0010 (m/s/($\sqrt{s}$)))
Accel internal quantization	2.70E-03 (counts to m/s)	2.70E-03 (counts to m/s)	2.70E-03 (counts to m/s)
Accel external quantization	5.00E-05 (counts to m/s)	7.50E-05 (counts to m/s)	1.00E-04 (counts to m/s)

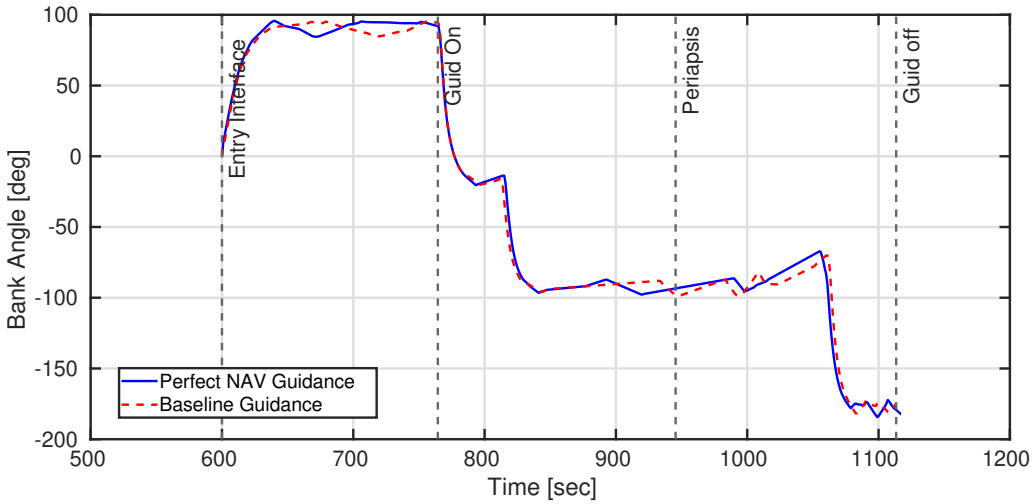

Fig. 3 FNPAG Bank Commands using perfect navigation (navigation) states vs. baseline simulation with onboard navigation errors.

Figure 3, for both cases, FNPAG stays in phase one for approximately the same time. During this phase, the FNPAG tries to solve for the switching time [16] , and one can see from Figure 3 that FNPAG's switching time solution for both cases are similar and are at about 810 sec. Similarly, during phase two [16] of the FNPAG, similar bank commands are issued in both cases. This shows us that for the baseline case that uses the highest quality IMU, the effect of the onboard navigation errors on the guidance is comparable.

Once the FNPAG commands are issued, the vehicle's control systems will track the guidance commands using these commands and the current onboard navigation states. Here, there are two sources of errors—the errors in the FNPAG commands and the sensed onboard current navigation states. Figure 4 compares the aerocapture trajectory and performance of the baseline simulation with the aerocapture trajectory using the perfect onboard navigation states. The top left plot in Figure 4 shows the variation of the inertial velocity with respect to the geodetic altitude. The top right figure shows the change in the eccentricity. For both cases, the aerocapture enables the vehicle to capture into an orbit from a hyperbolic trajectory. The bottom left plot shows the Sutton-Graves convective heating and the total heat load that the vehicle experiences during aerocapture. The bottom right plot shows the vehicle's sensed accelerations during the aerocapture. As one can see, the aerocapture trajectory and its performance are very similar for both cases. This

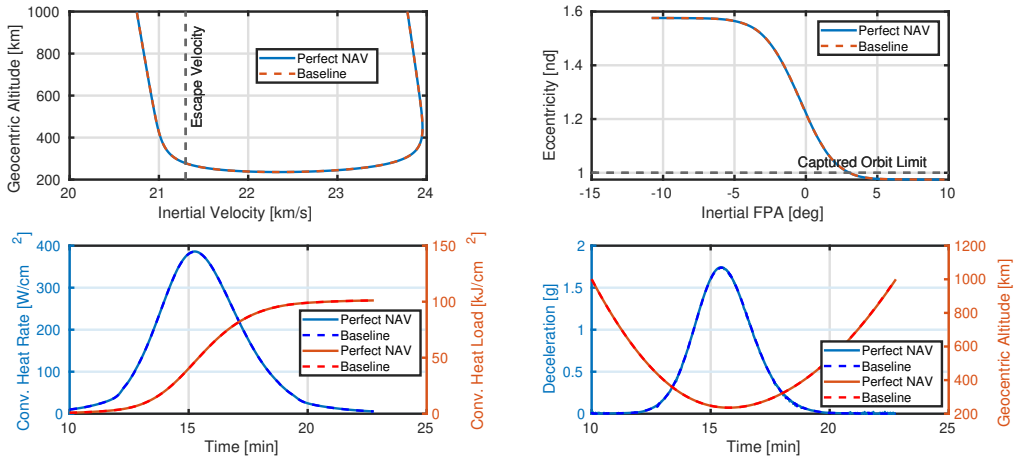

Fig. 4 Aerocapture trajectory: perfect navigation (navigation) states vs. baseline simulation with onboard navigation errors.

shows that for the baseline case, the effect of the onboard navigation errors that get passed on to other GNC subsystems does not significantly change the aerocapture trajectory or its performance.

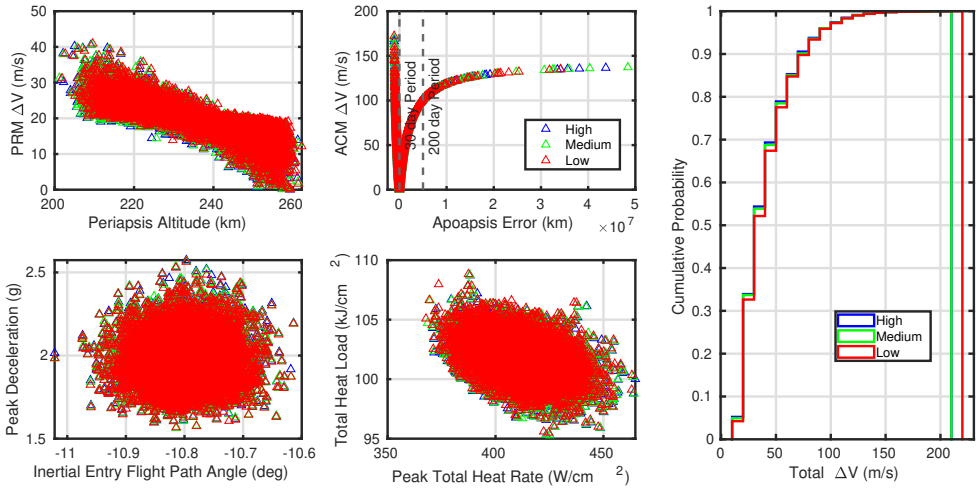

Fig. 5 Sensitivity of IMU quality on the aerocapture performance.

Figure 5 shows the sensitivity of the IMU quality with respect to the aerocapture performance. This study's high, medium, and low-quality IMU specifications correspond to the Orion-class, MIMU-class, and LN-200 Class IMU specifications. Figure 5 compares the aerocapture performance using different quality IMUs. Specifically, the plots show the ΔV required to raise to the target periapsis, which is 53000 km as a function of post aerocapture orbit's periapsis, and also shows the ΔV required at the target periapsis to target the desired apoapsis as a function of the apoapsis error. In addition, these plots show the maximum sensed acceleration seen in three cases as a function of the inertial entry flight path angle, and show the Sutton-Graves total heat load as a function of the maximum heat rate. Figure 5 also shows the cumulative probability total ΔV required to get into the final desired orbit post-apocapture. As one can see, all three IMUs provide more or less similar aerocapture performance. However, as the cumulative probability plots present, the high-quality IMU has slightly more counts in the bins with smaller total ΔV, which corresponds to better aerocapture performance. This sensitivity study shows that the aerocapture performance improves marginally with the quality of the IMU, as expected. Therefore, improving the quality of the three space-qualified IMUs considered in this

study is not very sensitive to the aerocapture performance.

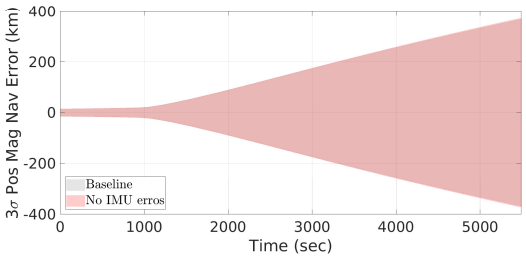

(a) Nav Error in position magnitude with no IMU errors

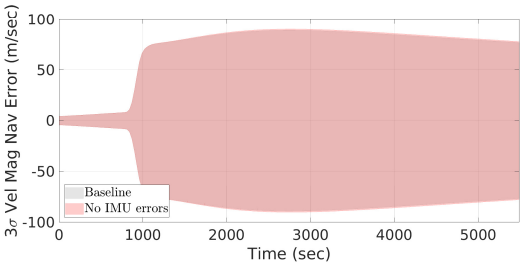

(b) Nav Error in velocity magnitude with no IMU errors

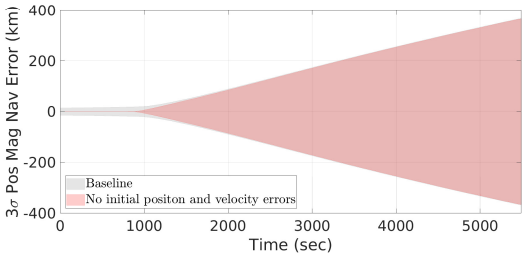

(c) Nav Error in position magnitude with no initial position and velocity errors

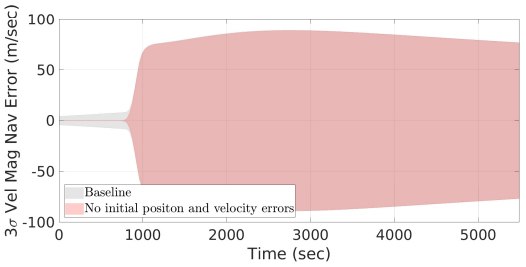

(d) Nav Error in velocity magnitude with no initial position and velocity errors

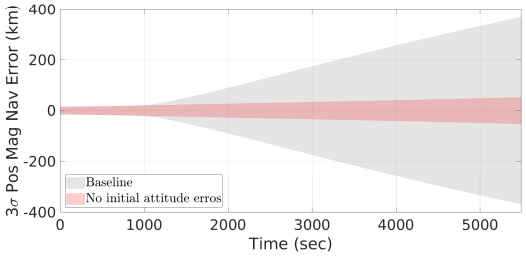

(e) Nav Error in position magnitude with no initial attitude error

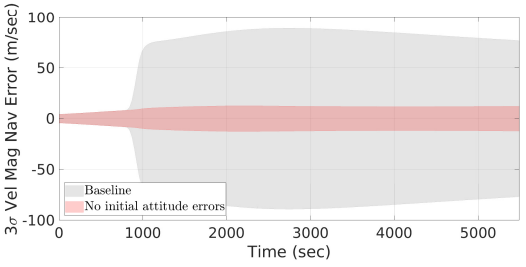

(f) Nav Error in velocity magnitude with no initial attitude error

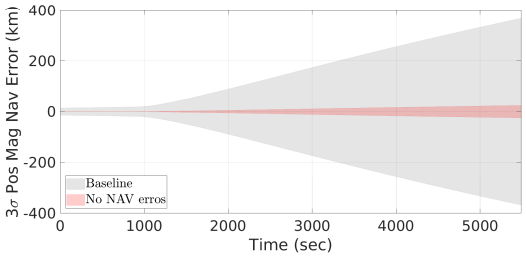

(g) Nav Error in position magnitude with no initial position, velocity, attitude and IMU errors

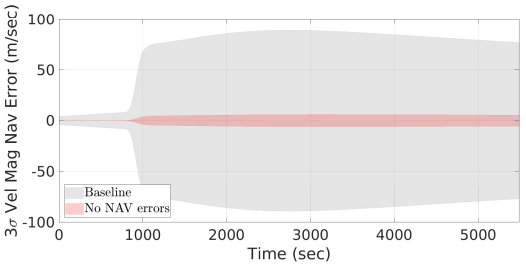

(h) Nav Error in velocity magnitude with no initial position, velocity, attitude and with IMU errors

Fig. 6 Contribution of different sources to the onboard navigation errors during aerocapture

An 8001 case Monte Carlo analysis is performed for each simulation setting to compute the navigation error standard deviation. Figure 6 shows how the three standard deviation (3σ) of navigation errors grow for an aerocapture trajectory with different simulation settings. From these 8001 aerocapture trajectories, navigation errors are sampled every 30 seconds along the trajectory. Using these samples, the standard deviation of the navigation errors at 30-second intervals along the trajectory are generated along the aerocapture trajectory. The plots in Figure 6 compare the 3σ navigation errors of the baseline simulation with the cases: 1) when there are no IMU errors; 2) when the MEKF filter is initialized with the same position and velocity as the truth states; 3) when the MEKF filter attitude states are initialized same as the

truth states and 4) when there are no IMU errors and with same initial position, velocity, and attitude for the MEKF compared to the truth states. Neither the IMU errors nor the different initial position and velocity states for the MEKF contribute considerably to the navigation errors. On the other hand, having the same initial attitude for the MEKF compared to the truth states reduced the navigation error significantly compared to the baseline case. The case with no IMU errors and the same initial MEKF states as the truth states should ideally have no navigation errors. However, small navigation errors arise as the MEKF estimates the onboard states using the discrete IMU measurements. These estimates will deviate from the truth states, especially when the dynamics are fast, which is true when the vehicle flies through a dense atmosphere during the aerocapture. This analysis shows the navigation errors will increase over time with no measurement updates. Further, it shows that the navigation errors are highly susceptible to errors in the initial attitude estimate of the MEKF.

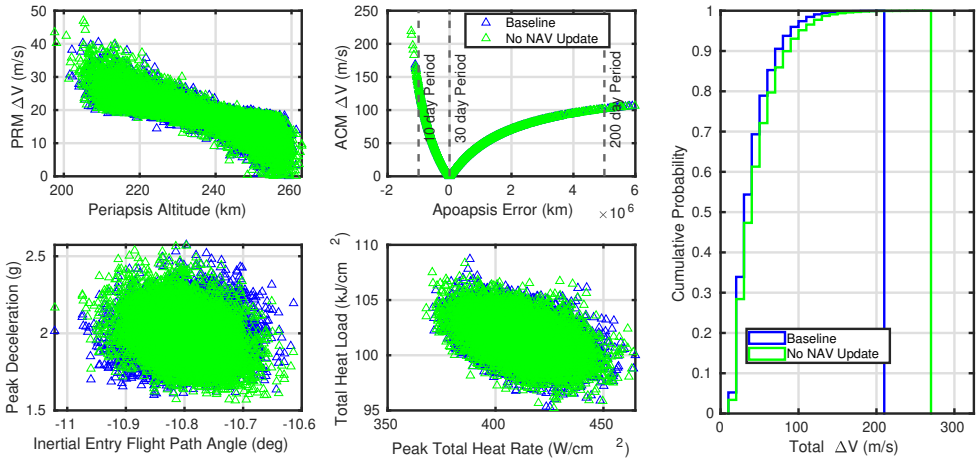

Fig. 7 Sensitivity of navigation update on the aerocapture performance.

Figure 7 compares the aerocapture performance of the baseline simulation with a scenario in which the spacecraft does not receive a navigation update in the 16 hours prior to entry, as discussed in Section II.A.1. The plots in Figure 7 are similar to those in Figure 5. The lack of a navigation update causes higher navigation errors in the system. However, the aerocapture performance with no navigation update is comparable to the baseline simulation, as shown in Figure 7. From the cumulative probability plot of the total ΔV to insert into the desired orbit post-aerocapture, it is apparent that the performance degrades with no navigation update, though the magnitude of degradation shows the system is not very sensitive to the navigation update.

B. LinCov Analysis

This section shows the 3σ results of the navigation error analysis and compares it with the values from POST2. For this comparison to be reasonable, the Monte Carlo runs in POST2 assumed no errors in the initial attitude and no quantization errors. Furthermore, the guidance and control subsystems are run using the POST2 truth states for this comparison, and this way, the navigation errors are mainly due to the noisy IMU measurements and the MEKF process noise and propagation errors. Table 4 and Table 5 shows the navigation error at atmosphere exit + 10 minutes. As expected, navigation errors increase when a lower-quality IMU is used. The results from POST2 are obtained using the sample covariance from the Monte Carlo runs. Overall, the LinCov results are close to the POST2 navigation analysis done using the sample covariance except for the velocity components of the low-quality IMU. Like the sensitivity study of IMU quality from POST2, LinCov presents similar navigation errors for each IMU with a different quality.

IV. Conclusions

This paper studies the onboard navigation errors during the aerocapture at Uranus. During aerocapture, one can expect no measurement updates other than IMU measurements. As IMU measurements have some inherent noise, the onboard navigation errors increase with time. These errors significantly increase when the dynamics are fast, which is the case when the vehicle flies through a dense atmosphere during the aerocapture. This work shows that the effect of

Table 4 3σ results of the position navigation error analysis from LinCov vs. POST2

Parameter	Low quality		Med quality		High quality	
	LinCov	POST2	LinCov	POST2	LinCov	POST2
Pos X (km)	14.030	12.4670	14.001	6.5594	13.910	5.6824
Pos Y (km)	9.273	7.5244	9.269	5.8389	9.228	5.7349
Pos Z (km)	23.912	26.4292	23.819	24.3311	23.577	24.1155
Pos Mag (km)	29.2334	30.1753	29.1421	25.8673	28.8878	25.4310

Table 5 3σ results of the velocity navigation error analysis from LinCov vs. POST2

Parameter	Low quality		Med quality		High quality	
	LinCov	POST2	LinCov	POST2	LinCov	POST2
Vel X (/secm)	7.910	27.4532	7.447	10.4081	7.431	6.1594
Vel Y (m/sec)	7.238	8.2594	7.110	4.9871	6.840	4.6212
Vel Z (m/sec)	11.774	24.8231	11.540	11.7815	11.412	9.2602
Vel Mag (m/sec)	15.9243	37.9220	15.4655	16.4925	15.2394	12.0434

onboard navigation errors on the guidance and control sub-systems to perform aerocapture is reasonable. The analysis in this study indicates that the three space-qualified IMUs, Orion class, MIMU class, and LN-200 class IMUs, provide similar aerocapture performance. This study also shows that not having the initial attitude the same as the truth states for the onboard filter is the primary source of onboard navigation errors. In addition, this work shows that the aerocapture performance degrades reasonably when the vehicle does not get a navigation update 16 hours before the entry. The onboard navigation analysis performed in POST2 is verified and validated in LinCov. The LinCov results closely match the POST2 navigation analysis for medium and high-quality IMUs. For the low-quality IMU, the LinCOV position errors and POST2 position errors match closely, but POST2 shows more error in the velocity compared to the LinCov analysis. Sensitivity analysis from both POST2 and LinCov shows that the aerocapture performance is less sensitive to the quality of the three space-qualified IMUs considered in this work.

References

[1] Dutta, S., Shellabarger, E., Scoggins, J., Gomez-Delrio, A., R.A., L., R.G., D., Chadalavada, P., Williams, J., Garland, J., Johnson, B., Matz, D., Geiser, J., Morgan, J., Restrepo, R., and Mages, D., "Uranus Flagship-class Orbiter and Probe using Aerocapture," *AIAA SciTech,* Orlando, FL, 2024.

[2] Lockwood, M., "Aerocapture Systems Analysis for a Neptune Mission," Tech. rep., NASA TM 2006-214300, 2006.

[3] Dutta, S., "Aerocapture Solutions for Flagship-class Uranus Orbiter and Probe," *AIAA SciTech Conference,* Orlando, FL, 2025.

[4] Justh, H. L., Cianciolo, A. M., Hoffman, J., and Allen, G. A., "Uranus Global Reference Atmospheric Model (Uranus-GRAM): User Guide," Tech. rep., TM 2021-0017250, 2021.

[5] Deshmukh, R., Dutta, S., Lugo, R., Restrepo, R., Mages, D., Johnson, B., Matz, D., Geiser, J., Scoggins, J. B., Shellabarger, E., Gomez-Delrio, A., and Williams, J., "Performance Analysis of Aerocapture Systems for Uranus Orbiter," *AIAA SciTech,* Orlando, FL, 2024.

[6] Shellabarger, E., Scoggins, J., Hinkle, A., Dutta, S., Deshmukh, R., Patel, M., and Agam, S., "Aerodynamic Implications of Aerocapture Systems for Uranus Orbiters," *AIAA SciTech,* Orlando, FL, 2024.

[7] Shellabarger, E., "Aerodynamics of a Uranus Aerocapture System using a Mars-Heritage Entry Vehicle," *AIAA SciTech Conference,* Orlando, FL, 2025.

[8] Mages, D., Restrepo, R., R.G., D., and Benhacine, L., "Mission Design and Navigation Solutions for Uranus Aerocapture," *AIAA SciTech,* Orlando, FL, 2024.

[9] Mages, D., Restrepo, R., Chadalavada, S., Deshmukh, R., Dutta, S., and Benhacine, L., "Mission Design and Navigation for Uranus Aerocapture Leveraging Super Heavy-Lift Launch Vehicles," *AIAA SCITECH 2025 Forum*, 2024.

[10] Jang, B. S. F. M. W. D. M. D. B. E., J. W., and Hannan, M., "Linear Covariance Analysis for a Lunar Lander," *AIAA SCITECH 2017 Forum*, 2017.

[11] James Williams, D. W., William E. Brandenburg, and Putnam, Z. R., ""Validation of Linear Covariance Techniques for Mars Entry, Descent, and Landing Guidance and Navigation Performance Analysis," *AIAA SCITECH 2022 Forum*, 2022.

[12] Evans, S., Taber, W., Drain, T., Smith, J., Wu, H.-C., Guevara, M., Sunseri, R., and Evans, J., "MONTE: the next generation of mission design and navigation software," *CEAS Space Journal*, Vol. 10, 2018, pp. 79–86.

[13] Restrepo, R., Mages, D., Deshmukh, R., Dutta, S., and Benhacine, L., "Mission Design and Navigation Solutions for Uranus Aerocapture," *AIAA Paper*, 2024.

[14] Deshmukh, R., "6-DOF Uranus Aerocapture Trajectory Analysis," *AIAA SciTech Conference,* Orlando, FL, 2025.

[15] Striepe, S., Powell, R., Desai, P., Queen, E., Way, D., Prince, J., Cianciolo, A., Davis, J., Litton, D., Maddock, R., Shidner, J., Winski, R., O'Keefe, S., Bowes, A., Aguirre, J., Garrison, C., Hoffman, J., Olds, A., Dutta, S., Zumwalt, C., White, J., Brauer, G., Marsh, S., and Engel, M., *Program To Optimize Simulated Trajectories II (POST2), Vol. II: Utilization Manual,* Version 3.0.NESC, 2015.

[16] Sandoval, S., "A Comparison of Bank Control and Direct Force Control for Aerocapture at Uranus," *AIAA SciTech Conference,* Orlando, FL, 2025.

[17] Dwyer-Cianciolo, A. M., Karlgaard, C. D., Woffinden, D., Lugo, R. A., Tynis, J., Sostaric, R. R., Striepe, S., Powell, R., and Carson, J. M., "Defining Navigation Requirements for Future Missions," *AIAA SciTech,* San Diego, CA, 2019.